

# A new method to estimate dark matter halo concentrations

Christian Poveda<sup>1</sup> & Jaime E. Forero-Romero<sup>1</sup>

<sup>1</sup>*Departamento de Física, Universidad de los Andes, Cra. 1 No. 18A-10, Edificio Ip, Bogotá, Colombia*

23 January 2015

## ABSTRACT

asd

**Key words:** methods: numerical, galaxies: haloes, cosmology: theory, dark matter

## 1 INTRODUCTION

In the concordance cosmology paradigm the the matter content of the Universe is dominated by dark matter which behaves as a collisionless fluid under the influence of gravity. In the last three decades numerical experiments have made possible the simulation of dark matter dominated universes, yielding valuable insights on the large scale structure formation process as depicted in observations.

One of the most striking results of these simulations is that dark matter clumps on galactic scales follow a universal density profile which in a first approximation is spherical symmetric and only dependent on the radial coordinate. These profiles seem to be universal; independent of the cosmological parameters and self-similar for different spatial scapes after an addequate re-scaling is applied.

One the most common parameterization of this density is known as the Navarro-Frenk-White (NFW) profile (Navarro et al. 1997). This profile is a double power law in radius, where the transition between the two happens at the so-called scale radius  $r_s$ . The ratio between the scale radius and the virial radius of the halo  $R_v$  is known as the concentration  $c = R_v/r_s$ , a quantity that has been found to be correlated with the halo mass.

The relationship between halo mass and concentration is in principle accesible to observations and provides a potential test of LCDM on galactic scales. With this promise a great deal of effort has been invested in calibrating this relationship with simulations but also finding the best possible way to constraint it with observations.

From the computational point of view there are two main methods to estimate the concetration parameter of a dark matter halo in a N-body simulation. The first method takes the particles composing the halos and bins them in logarithmic radii to estimate the density in each bin, then it proceeds with a fit of this density estimation as a function of radius. A second method uses an analytical property of the NFW that related the maximum of the ratio of the circular velocity to the virial velocity. In this method at each particle radius this ratio is estimated to find the maximum value for

this ratio; this value is used to find the roots of an equation which represent the concentration parameter.

The first method although is straightforward to apply has two main disadvantages. First of all it requires a large number of particles in order to have a proper density estimate in each bin. For a very low number of particles is hard to define a large number of bins to proceed with the fit. The second problem is that, as in any process involving data binning, there is not an way to estimate the optimal bin size, which in turn can affect the results of the fit.

The second method solves the two problems mentioned above. It works with low particles numbers and does not involve data binning. However, it effectively takes into account a single data point and discards the behaviour of the ratio  $V_{circ}/V_{vir}$  below and above its maxima.

In this paper we propose a new method to estimate the dark matter halo concentration from N-body simulation results. This method has two advantages with respect to the methods mentioned above. First, it does not involve data binning. Second, it does not throw away data points. Third, it allows for an straightforward estimation of the uncertainties in the concentration parameter.

Our method consists in building the cumulative mass profile from the particle data in the N-body simulation to find the best possible concentration value using a Markov Chain Monte Carlo methodology by comparing the data against the analytical expectation.

This paper is structured as follows. In Section 2 we review the basic properties of the NFW density profile and define the basic notation for the rest of the paper. Next in Section 3 we present our new method to estimate the halo concentration, payin special attention to the bayesian framework to find the most probable value and its uncertaintt. In Section ?? we demonstrate the power of our method with two different halo samples; the first one generated under controlled conditions and the second taken from a cosmological N-body simulation. Next in ?? we discuss these results by comparing them against other methods to estimate the concentration and comment on the consequences for the

concentration-mass relationship. We present our conclusions in Section 5.

## 2 BASIC PROPERTIES OF THE NFW DENSITY PROFILE

### 2.1 Density profile

The NFW density profile can be written as

$$\rho(r) = \frac{\rho_c \delta_c}{r/r_s (1 + r/r_s)^2}, \quad (1)$$

where  $\rho_c \equiv 3H^2/8\pi G$  is the Universe critical density,  $\delta_c$  is the halo dimensionless characteristic density and  $r_s$  is known as the scale radius, the radius that marks the transition between the power law scaling  $\rho \propto r^{-1}$  for  $r < r_s$  and  $\rho \propto r^{-3}$  for  $r > r_s$ .

We define the virial radius of a halo,  $r_v$ , as the boundary of the spherical volume that encloses a density of  $\Delta_h$  times the average density of the Universe. The corresponding mass  $M_v$ , the virial mass, can be written as  $M_v = \frac{4\pi}{3} \bar{\rho} \Delta_h r_v^3$ .

### 2.2 Integrated Mass

From these definitions we can compute the total mass enclosed inside a radius  $r$ :

$$M(< r) = 4\pi \rho_c \delta_c r_s^3 \left[ \ln \left( \frac{r_s + r}{r} \right) - \frac{r}{r_s + r} \right]. \quad (2)$$

We express the same quantity in terms of dimensionless variables  $x \equiv r/r_v$  and  $m \equiv M(< r)/M_v$ ,

$$m(< x) = \frac{1}{A} \left[ \ln(1 + xc) - \left( \frac{xc}{xc + 1} \right) \right], \quad (3)$$

where

$$A = \ln(1 + c) - \left( \frac{c}{c + 1} \right), \quad (4)$$

and the parameter  $c$  is known as the concentration  $c \equiv r_v/r_s$ .

From this normalization value and for later convenience we define the following function

$$f(x) = \ln(1 + x) - \left( \frac{x}{x + 1} \right). \quad (5)$$

The most interesting feature of Eq. (3) is that the concentration is the only free parameter to describe the density profile. In Figure 1 we show  $m(< x)$  as a function of  $x$  for different values of the concentration in the range  $1 \leq c \leq 20$ .

### 2.3 Circular velocity

It is also customary to express the mass of the halo in terms of the circular velocity  $V_c = \sqrt{GM(< r)/r}$ . From this we can define a new dimensionless circular velocity  $v(< x) \equiv V_c(< r)/V_c(< r_v)$ , using the result in Eq. 3 to have:

In Figure 2 we show the circular velocity profile for the same concentrations as in Figure 1.

$$v(< x) = \sqrt{\frac{1}{A} \left[ \frac{\ln(1 + xc)}{x} - \frac{c}{xc + 1} \right]}, \quad (6)$$

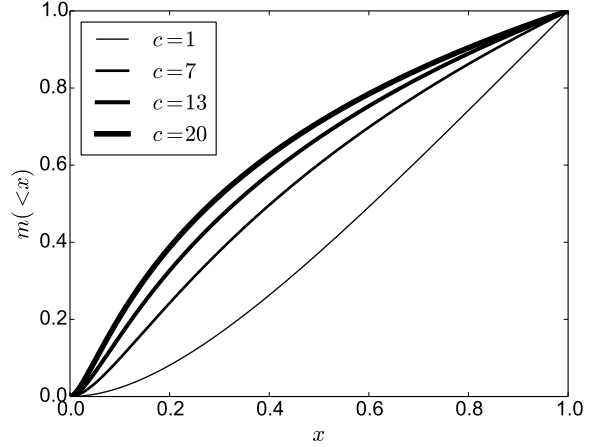


**Figure 1.** Dimensionless mass profiles as a function of the dimensionless radius for different concentration values.

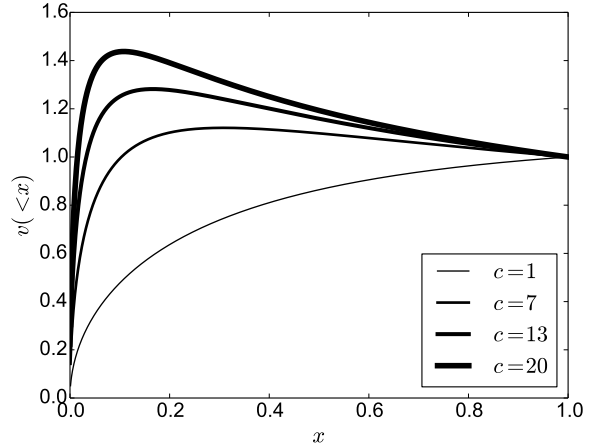


**Figure 2.** Dimensionless velocity profiles as a function of the dimensionless radius for different concentration values.

this normalized profile always shows a maximum provided that the concentration is larger than a values of  $c > ???$ . It is possible to show that for the NFW profile the maximum is provided by

$$\max(v(< x)) = \sqrt{\frac{c}{x_{\max}} \frac{f(x_{\max})}{f(c)}}, \quad (7)$$

where  $x_{\max} = 2.163$  and the function  $f(x)$  was defined in Eq. (5).

## 3 A NEW APPROACH TO ESTIMATE THE HALO CONCENTRATION

As we saw in the previous sections, once the density profile is expressed in dimensionless variables the only free parameter in the density profile is the concentration. There are two

main methods to estimate concentrations in dark matter halos extracted from N-body simulations.

The first method tries to directly estimate the density profile. It takes all the particles in the halo and bins them in the logarithm of the radial coordinate from the halo center. Then, it estimates the density in each logarithmic bin counting the particles and dividing by the corresponding shell volume. At this point it is possible to make a direct fit to the density as a function of the radial coordinate. This method has been most recently used by Ludlow et al. (2014) to study the mass-concentration-redshift relation of dark matter halos using the Millennium Simulation Series.

A second method uses the circular velocity profile. As it was shown in Fig. (2) the circular velocity shows a maximum for all profiles with concentration values larger than  $c > 2$ . The method finds the value of  $x$  for which the normalized circular velocity  $v(< x)$  shows a maximum. Using this value it solves numerically for the corresponding value of the concentration using Eq. (7). This method has been most recently used by Klypin et al. (2014) to study the mass-concentration-redshift relation using the Multidark Simulation Suite.

Our method is a third option that uses the integrated mass profile. First we define the center of the halo to be at the position of the particle with the lowest gravitational potential. Then we rank the particles by their increasing radial distance from the center. From this ranked list of  $i = 1, N$  particles, the total mass at a radius  $r_i$  is  $M_i = i \times m_p$ , where  $r_i$  is the position of the  $i$ -th particle and  $m_p$  is the mass of a single computational particle. In this process we discard the particle at the center.

We stop the construction of the integrated mass profile once we arrive at an average density of  $\Delta_h \bar{\rho}$ , with  $\Delta_h = 740$ , roughly corresponding to 200 times the critical density. This radius marks the virial radius and the virial mass. We divide the enclosed mass  $M_i$  and the radii  $r_i$  by these virial values to obtain the dimensionless variables  $m_i$  and  $x_i$ .

The construction of the numerical integrated mass profile has the advantage that it does not involve any binning and uses the information from all the particles in the halo, unlike the method that tries to directly build. Furthermore, as it will be clear in the next paragraph, the fit of this computational profile to the analytic expectation uses the information from all points, not only a single maxima point as the method using the circular velocity profile.

We use a Metropolis-Hastings algorithm to sample the likelihood function distribution defined by  $\mathcal{L}(c) = \exp(-\chi^2(c)/2)$  where the  $\chi^2(c)$  is written as

$$\chi^2(c) = \sum_{i=1}^N [\log m_i - \log m(< x_i; c)]^2, \quad (8)$$

where  $m(< x_i; c)$  corresponds to the values in Eq.(3) at  $x = x_i$  for a given value of the concentration parameter  $c$  and the  $i$  index sums over all the particles in the numerical profile.

For the walk in the Metropolis-Hastings algorithm we used 50000 steps where each step was randomly generated with a normal distribution centered around the last step with a standard deviation of  $\sigma = 0.03$ . From the  $\chi^2$  distribution we find the optimal value of the concentration and its associated uncertainty.

## 4 RESULTS

In this Section we present the results of applying our method on two different halo samples.

The first sample is composed by mock halos generated to have known concentration values in perfect spherical symmetry following an NFW profile. We use this sample to check that we can recover the expected values but also gauge the impact of the number of particles on the outcomes and the difference with respect to the two other fitting methods.

The second sample comes from a publicly available N-body cosmological simulation. From this sample we quantify again the differences between all the methods we have to fit the data. We also estimate the possible impact of the different methods in estimating the mass-concentration relationship from simulations.

### 4.1 Tests on Mock Halos

The method we use to generate the halos is based on the integrated mass profile. We start by fixing the desired concentration  $c$  and total number of particles  $N$  in the mock halo. With this values we define the mass element as  $\delta m = 1/M$ , corresponding to the mass of each particle such that the total mass is one. Then for each particle  $i = 1, \dots, N$ , we find the value of  $r_i$  such that the difference

$$m(< r_i; c) - i \cdot \delta m \quad (9)$$

is zero using Ridders' method.

The value of  $r_i$  is the radius of the  $i$ -th particle of the mock halo. Then we generate random polar and azimuthal angles  $\theta$  and  $\phi$  for each particle to ensure spherical symmetry. Finally these three spherical coordinates are transformed into cartesian coordinates  $(r, \theta, \phi) \rightarrow (x, y, z)$ .

We generate in total 400 mock halos splitted into four different groups of 100 halos each. The four groups differ in the total number of particles for their halos: 20, 200, 2000 and 20000. Inside each group the halos have random concentration values in the range  $1 < c < 20$  with a flat distribution. For all these halos we find the concentration values using the density, velocity and mass methods described in the previous section. We quantify the difference between the expected  $c_{in}$  and obtained  $c_{out}$  values by

$$D = (c_{in} - c_{out})/c_{in}. \quad (10)$$

#### 4.1.1 The impact of particle number

Figure 3 shows the integrated distribution for  $D$  for the fits using our method, splitted into four different groups according the particle number. From this Figure the first immediate conclusion is that increasing the number of particles increases the chances to recover the input values.

We believe that the main effect that contributes to this trend is that the particle that our algorithm finds to be the halo center (where the potential is minimum) gets closer to the original geometrical center (where no particle sits by construction) used to generate the halo. Poissonian noise makes this center fluctuate, changing the numerical radial profile from the analytical input.

For particle number of 20 the offset between the input

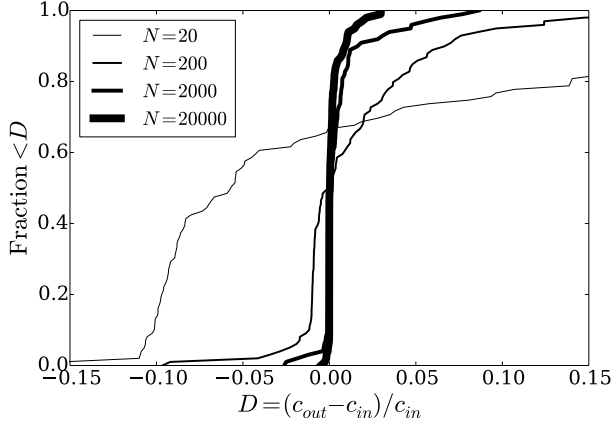


**Figure 3.** Cumulative distribution of the fractional difference,  $D$ , between the input concentration in the mock halo generator,  $c_{in}$  and the measurement by our MCMC code,  $c_{out}$ . Each curve corresponds to halos generated with a different number of particles,  $N$ .

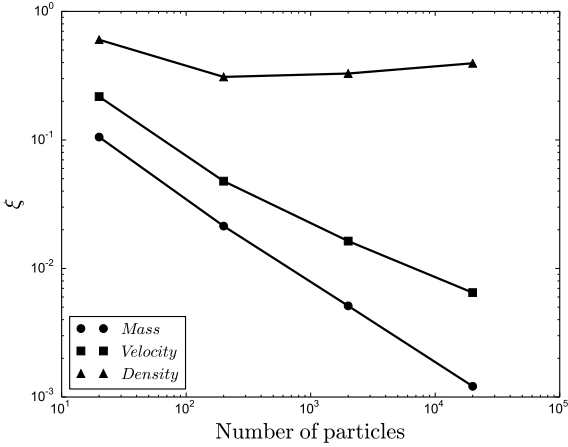


**Figure 4.** Average value of the relative error in the concentration estimate,  $\langle |D| \rangle$ , as a function of the particle number  $N$  in the set of mock halos. Different symbols represent different methods. Our method provide the most accurate estimate at fixed particle number  $N$ .

and output concentration can be as large as 20%, with a slight bias around  $-0.05\%$ , i.e. the output concentration is biased towards lower values than the input. For particle numbers of 2000 most of the offsets fall below 5%, with a clear peak around 0% indicating that any appreciable bias is absent.

#### 4.1.2 The impact of the input concentration

Hace falta hacer una figura para este caso.

#### 4.1.3 The impact of different methods

Using this dataset we also compare our method against the other two methods described earlier: using shells to esti-

mate the density as a function of radius and the maximum circular velocity method. In the first case we use the same Metropolis-Hastings algorithm we have in our method to fit the density profile. In the second method we simply follow the procedure described in Section 3

We quantify the accuracy of each method with the following statistic:

$$\langle |D| \rangle = \frac{1}{|\mathcal{H}_N|} \sum_{\mathcal{H}_N} |D|, \quad (11)$$

where  $\mathcal{H}_N$  corresponds to the set of haloes with  $N$  particles,  $D$  follows the definition in Eq. (10) and  $|\mathcal{H}_n|$  is the number of haloes in  $\mathcal{H}_n$ .

Figure 4 shows the behaviour of  $\langle |D| \rangle$  as a function of halo particle number for the three different methods to estimate the concentration. At fixed particle numbers our method always shows the lowest  $\langle |D| \rangle$  values compared to the other two methods. Its accuracy is on the order of 10% for 20 particles in the halo, going down to 0.1% for halos with 20000 particles. The decrease of  $\langle |D| \rangle$  with increasing particle number  $N$  goes approximately as  $\langle |D| \rangle \propto N^{-1/2}$ , which reinforces the hint that the accuracy of the method is related to a decrease of Poissonian noise.

The second best accuracy is achieved by the method based on the maximum of the circular velocity. It also shows a similar behaviour  $\langle |D| \rangle \propto N^{-1/2}$ . Its accuracy is 2–5 times less than in our method, on the order of 20% for 20 particle halos and 0.5% for 20000 particle halos. The method based on the direct density fit shows the lowest accuracy of all methods. Its average values  $\langle |D| \rangle$  are always between 30% and 50% regardless of the particle number. **Necesitamos entender el comportamiento de esto.**

## 4.2 Tests on N-body data

We use data from the MultiDark cosmological simulation. It follows the non-linear evolution of a dark matter density field sampled with  $2048^3$  particles over a cubic box of  $1000 h^{-1} \text{Mpc}$  on a side. The data is publicly available through <http://www.cosmosim.org/>. More details about the structure of the database and the simulation can be found in (Riebe et al. 2013).

We build a sample of all halos located in a cubic sub-volume of  $100 h^{-1} \text{Mpc}$  on a side centered on the most massive halo in the simulation at  $z = 0$  which corresponds to the **miniMDR1** tables in the database. From this sample we select all the halos at  $z = 0$  detected with a Friends-of-Friends (FoF) algorithm with masses in the interval  $10^{11} \leq M_{\text{FoF}}/h^{-1} \text{M}_{\odot} \leq 10^{15}$ . The FoF algorithm used with a linking length of 0.17 times the average interparticle distance. This choice translates into an overdensity  $\Delta_h \sim 400 - 700$  dependent on the halo concentration (More et al. 2011). Finally, for each FoF halo we select from all the particles that belong to it.

From this set of particles we follow the procedure spelled out in Section 3 with  $\Delta_h = 740$  (corresponding to 200 times the critical density) to find the halo concentration. This choice makes that our overdensities are fully included inside the original FoF particle group. We only report results from overdensities with at least 100 particles. Finally, we

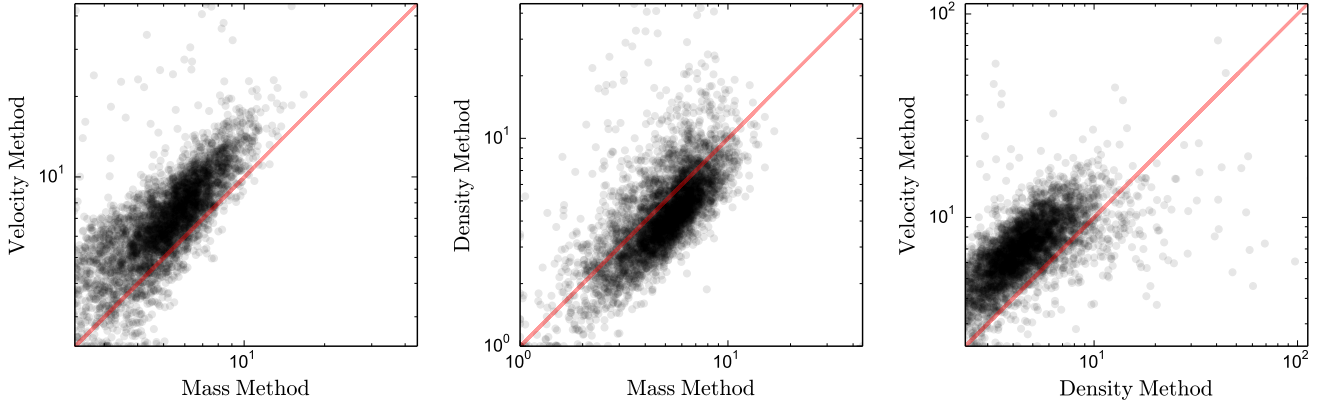


**Figure 5.** Comparison between the obtained concentrations by the three methods

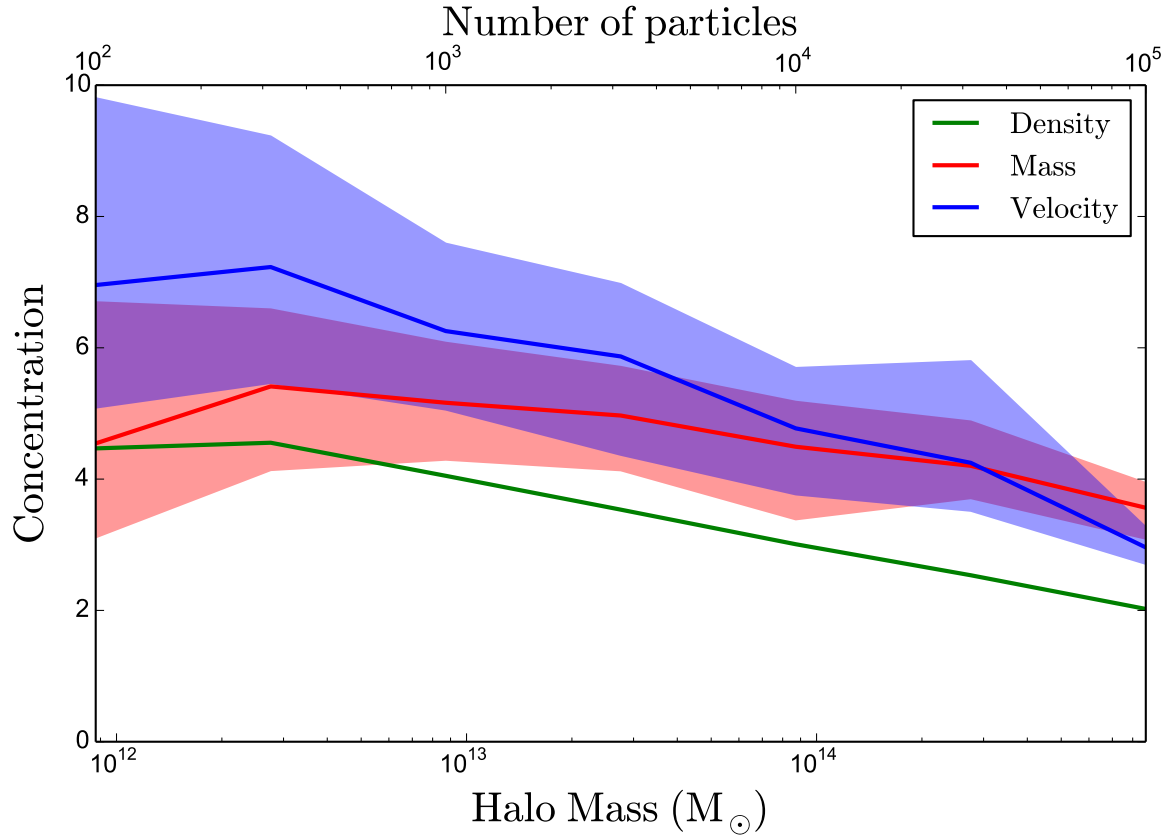


**Figure 6.** Mass-concentration relationship for the three different methods used on the same cosmological N-body data. The central lines correspond the median and the shadowed region indicates the quartiles.

store the values obtained for the virial radius, virial mass and concentration.

Figure 5 shows the results that compare the concentration values in the simulated halos from the three different methods. At zeroth order the results are consistent. However, the concentration values from the velocity method produces concentrations that are  $XXX$  times larger on average than the results from our method. On the other hand, the

concentrations from the velocity method are  $XXX$  times lower than in our method.

Figure ?? shows the mass-concentration relationship from the N-body data with the results of the three different methods. The central lines correspond the median and the shadowed region indicates the quartiles. In this relationship our methods represents a compromise between the velocity and density methods. The slope is flatter and the overall

normalization is below the velocity method and above the density.

## 5 CONCLUSIONS

## REFERENCES

- Klypin A., Yepes G., Gottlober S., Prada F., Hess S., 2014, ArXiv e-prints
- Ludlow A. D., Navarro J. F., Angulo R. E., Boylan-Kolchin M., Springel V., Frenk C., White S. D. M., 2014, MNRAS, 441, 378
- More S., Kravtsov A. V., Dalal N., Gottlöber S., 2011, ApJS, 195, 4
- Navarro J. F., Frenk C. S., White S. D. M., 1997, ApJ, 490, 493
- Riebe K., Partl A. M., Enke H., Forero-Romero J., Gottlöber S., Klypin A., Lemson G., Prada F., Primack J. R., Steinmetz M., Turchaninov V., 2013, Astronomische Nachrichten, 334, 691
- <http://adsabs.harvard.edu/abs/2014ApJ...795...163U>
- <http://adsabs.harvard.edu/abs/2012ApJS...199...25P>
- Figura 3!